Spectroscopic characterization of photoinduced Mn^{5+} ions in $YAlO_3$

M. A. Noginov,* G. B. Loutts, and N. Noginova
Center for Materials Research, Norfolk State University, 2401 Corprew Avenue, Norfolk, Virginia 23504

S. Hurling and S. Kück
Institut für Laser-Physik, Jungiusstraße 9a, 20355 Hamburg, Germany

(Received 14 December 1998; revised manuscript received 11 June 1999)

We have spectroscopically studied the photoinduced color center in Mn:$YAlO_3$, the promising material for holographic data storage. We have proved that grayish-bluish coloration in photoexposed Mn:$YAlO_3$ is due to Mn^{5+} ions in octahedral sites. We assign the main features observed in the absorption and emission spectra of photodarkened Mn:$YAlO_3$ to the $^1T_2(t_2^2)$, $^3T_2(t_2e)$, $^3T_1(t_2e)$, $^1A_1(t_2^2)$, and $^3A_2(e^2)$ excited states of Mn^{5+}. We show that Mn^{5+} ions can be stabilized in Mn:$YAlO_3$ codoped with Ca ions and in the crystals grown in reducing atmosphere and subsequently annealed in air at 310–460 °C.

I. INTRODUCTION

The optical properties of Mn:$YAlO_3$ have been studied in the recent publications.[1,2] It has been shown that yellowish Mn:$YAlO_3$ (grown in the oxidizing atmosphere) under photoexcitation with green laser light changes the color to grayish or dark-grayish-bluish, depending on the exposure. Under photoexcitation of the sample with two mutually coherent laser beams an efficient diffraction grating, accompanying periodical photocoloration, is created in the crystal.[1,2] The long storage time of gray coloration (more than one year at room temperature) in combination with the possibility of quick fully reversible erasing of the coloration at >250 °C makes the crystal a promising material for holographic optical storage.[1,2]

As it was suggested in Refs. 1 and 2, the photoinduced color change of the crystal is due to photoionization of Mn^{4+} that is present in as grown $YAlO_3$ crystal ($Mn^{4+} \rightarrow Mn^{5+}$).[3]

The detailed spectroscopic study of different manganese valence states coexisting in $YAlO_3$ is necessary for better understanding of the mechanisms of photoinduced grating recording in the material. The properties of Mn^{2+}, Mn^{3+}, and Mn^{4+} ions in $YAlO_3$ have been discussed in detail in Refs. 4 and 5.

In the present work we study the photoinduced color center that is responsible for grayish-bluish coloration and conclude that its main spectroscopic properties correspond to those of Mn^{5+} in distorted octahedral environment. Our conclusion is based on:

(1) A good agreement between the energy positions of the experimentally observed spectroscopic features and those calculated according to the Tanabe-Sugano model;

(2) The absence of tetrahedral sites in $YAlO_3$;

(3) The obvious likeness of the absorption and emission spectra of photodarkened Mn:$YAlO_3$ with those of Mn^{5+} ions in tetrahedral coordination[6–9] and V^{3+} and Ti^{2+} ions in octahedral coordination.[10–15] (According to Ref. 6, spectroscopically there are apparent similarities between the octahedral and tetrahedral systems. Mn^{5+}, V^{3+}, and Ti^{2+} ions have the same electronic configuration, $3d^2$).

We found that under certain synthesis conditions (codoping of Mn:$YAlO_3$ with Ca and Ce ions or annealing in air of Mn:$YAlO_3$ crystal grown in reducing atmosphere) the grayish coloration in the samples is permanent (not erasable by heat). We show that characteristic permanent coloration in these crystals is also due to Mn^{5+} ions. The mechanisms of chemical stabilization of Mn^{5+} valence state in $YAlO_3$ are discussed.

In a large number of publications, tetragonally coordinated Mn^{5+} in different hosts was studied as a potential active ion for solid-state lasers. The laser operation of Mn^{5+} in $Ba_3(VO_4)_2$, $Sr_3(VO_4)_2$, and $Sr_5(VO_4)_3F$ has been reported by Merkle *et al.* in Refs. 16–18. Although, as we show in this paper, the emission in Mn:$YAlO_3$ is very weak, the spectroscopic study of Mn^{5+} in octahedral coordination in $YalO_3$ (which is complimentary to that in tetrahedral coordination in other crystals) can be of interest to the laser community.

II. EXPERIMENTAL SAMPLES AND TECHNIQUES

$YAlO_3$ is an orthorhombic crystal with the space group Pbnm.[19] YO_{12} polyhedron is strongly distorted with eight oxygen ions being located closer to Y^{3+} ions (average distance 2.28 Å) and four oxygen ions being further away at the average distance of 3.13Å. As a result of the distortion, the coordination number of Y^{3+} is close to 8 and the ionic radius of Y^{3+} in such coordination is equal to 1.019 Å.[20] Al^{3+} sites in $YAlO_3$ have almost ideal octahedral symmetry. As it has been discussed in Refs. 4 and 5, Mn^{4+} ions in Mn-doped $YAlO_3$ occupy Al site and Mn^{2+} ions occupy the Y site. In octahedral coordination the radius of Mn^{4+} ion is equal to 0.53 Å and in eightfold coordination the size of the Mn^{2+} ion is equal to 0.96 Å.[20] Apparently, Mn^{4+} ions provide charge compensation for Mn^{2+} ions, while some portion of Mn^{4+} content is compensated by traps.

The major part of experimental studies in this paper was done using Mn:$YAlO_3$ crystals grown (at the Center for Materials Research, Norfolk State University) in oxidizing, $N_2+0.2\%O_2$, atmosphere. As grown yellowish Mn:$YAlO_3$ crystals had high-optical quality. The concentration of Mn ions in the melt was equal to 0.5% and the concentration of Mn ions in the crystal was about 10% of that in the melt. The

detailed account of the crystal-growth procedure and the spectroscopic properties of Mn^{4+} ions (which determine yellowish coloration of as grown crystals) is given in Ref. 4. In this paper by saying Mn:$YAlO_3$ we mean the crystals grown in oxidizing atmosphere unless otherwise is stated.

Some of Mn:$YAlO_3$ samples were codoped with Ce, Ca, and Ce+Ca ions. As was shown in Ref. 5, the introduction of Ce ions to the crystal reduces the valence of Mn^{4+} ions to Mn^{3+}, apparently due to the reaction $Ce^{3+}+Mn^{4+} \rightarrow Ce^{4+}+Mn^{3+}$. As it will be shown in Sec. V, the codoping of the crystals with divalent Ca ions shifts manganese valence state to 5+.

We compared the properties of Mn:$YAlO_3$ samples grown in oxidizing atmosphere with those of a sample grown (at the Institute of Laser Physics, Hamburg University) in reducing atmosphere, $N_2+1\%H_2$. The optical quality of the crystals grown in reducing atmosphere was poorer than of those grown in oxidizing atmosphere. We found a significant difference between crystals grown in different conditions. The heating on a hot plate, which erases photoinduced gray coloration in the crystals grown in oxidizing atmosphere, produces an intense permanent gray coloration in the crystals grown in reducing atmosphere. In all the crystals manganese was added to the charge in the form of MnO_2.

In this paper, the polarized absorption measurements were carried out using the ultraviolet-visible-infrared spectrophotometer Cary 5G from Varian.

In the emission studies the crystals were excited with second harmonic of a *Q*-switched Nd:YAG laser (Quanta Ray-GCR-170) or cw Ar+ laser light. The emitted light was focused into a 0.46-m monochromator (Spex-HR 460). The long-pass glass filter was used to avoid second-order grating effects. The emission was searched in visible and near infrared ranges of the spectrum using a photomultiplier tube (S20 cathode) and $In_xGa_{1-x}As$ detector, respectively.

In low-temperature experiments the samples were immersed in liquid nitrogen or cooled in a helium cryostat to 14 K.

To erase photoinduced grayish coloration in the samples grown in oxidizing atmosphere and produce grayish coloration in the samples grown in the reducing atmosphere, we heat treated the crystals in air (on the hot plate) at 310–460 °C. The heat exposure in different experiments varied between 10 and 60 min.

III. EXPERIMENTAL RESULTS IN Mn:$YAlO_3$ GROWN IN OXIDIZING ATMOSPHERE

The absorption spectrum of strongly photoexposed dark grayish-bluish Mn:$YAlO_3$ crystal grown in oxidizing atmosphere is compared to that of yellowish (as grown or bleached) sample in Fig. 1. Six traces (1–6) in Fig. 1 correspond to three different orientations of light polarization **E** (along three crystallographic axes of the crystal) and two different light propagation directions for each polarization. The same spectra taken at liquid nitrogen temperature are given in the inset in Fig. 1. According to Ref. 4, six corresponding room-temperature absorption spectra of not exposed Mn:$YAlO_3$ are almost identical to each other. One of them is shown in Fig. 1, trace 7. As follows from Fig. 1, the absorption of illuminated sample is much more intense and

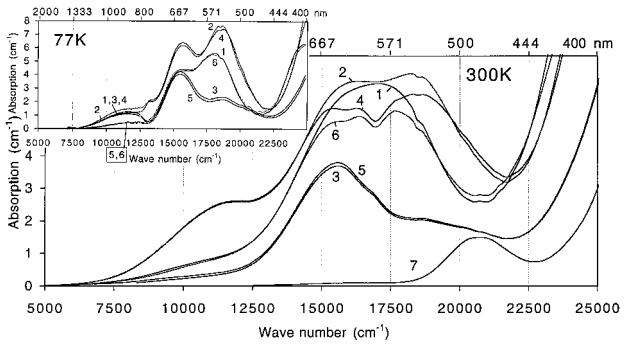

FIG. 1. Main frame: Traces 1–6-room-temperature absorption spectra of strongly photoexposed (at $\lambda=514.5$ nm) Mn:$YAlO_3$. 1–**k**‖**c**, **E**‖**a**, **H**‖**b**; 2–**k**‖**c**, **E**‖**b**, **H**‖**a**; 3–**k**‖**a**, **E**‖**c**, **H**‖**b**; 4–**k**‖**a**, **E**‖**b**, **H**‖**c**; 5–**k**‖**b**, **E**‖**c**, **H**‖**a**; 6–**k**‖**b**, **E**‖**a**, **H**‖**c** (where **a, b**, and **c** are the orthogonal crystallographic axes of the crystal and **k, E**, and **H** are the light propagation direction, polarization of the electric field, and polarization of the magnetic field, respectively). Trace 7–room-temperature absorption spectrum of the same not exposed crystal; **k**‖**c**, **E**‖**a**, **H**‖**b**. Inset: the same spectra in the exposed crystal at 77 K.

covers much wider spectral range than that of unexposed crystal. The main features in the absorption spectrum of Fig. 1 are listed in Table I. Note that the spectra corresponding to the same polarization of the electric vector **E** but different polarizations of the magnetic vector **H**, in general, do not coincide, see Fig. 1. This implies the presence of the magnetic dipole component in the absorption spectrum.

The absorption spectrum taken at 14 K reveals a weak and sharp peak at 1138 nm (8810 cm^{-1}) accompanied by several less intense Stokes and anti-Stokes lines, see Fig. 2.

Several weak sharp peaks at 20.57×10^3, 20.70×10^3, 24.43×10^3, and $21.95\times10^3\,cm^{-1}$ can be found in the low-temperature (77 K) absorption spectrum at **E**‖**a**. These peaks are shown with better resolution in Fig. 3.

In Mn:$YAlO_3$ there are two very strong-absorption bands ($K_{abs}^{max}\approx250\,cm^{-1}$) centered at ≈190 and 290 nm.[4] Both of them are apparently due to metal-oxygen charge transfer (CT).[21] In strongly photoexcited (dark grayish-bluish) samples the intensity of the 290-nm CT band reduces along with the reduction in Mn^{4+} concentration.[4] It has been concluded that this absorption band is partially due to $Mn^{4+}\rightarrow$oxygen CT or $Mn^{2+}\rightarrow$oxygen CT.[4] As follows from the absorption spectrum in Fig. 4, despite the reduction of the absorption intensity in the photoexposed sample in comparison with that in the unexposed sample at $>28\,000$ cm^{-1} (which is in accordance with Ref. 4), the absorption intensity in darkened crystal is stronger than that in unilluminated one between 21×10^3 and $28\times10^3\,cm^{-1}$. This implies that the 21×10^3-to-$28\times10^3\,cm^{-1}$ absorption in photodarkened sample is primarily not due to CT transitions but due to transitions between crystal field states of the same ion (we hint at Mn^{5+}) that is responsible for photocoloration of the crystal.

At the excitation of photoexposed Mn:$YAlO_3$ crystal with short light pulses ≈10 ns at 532 nm, the predominating emission signal is from Mn^{4+} ions. Mn^{4+} emission in $YAlO_3$, peaking at room temperature at 715 nm, was discussed in detail in Refs. 1, 2, and 4. At low temperatures, 14 and 77 K, very weak emission with the maximum at 1.14 μm was

TABLE I. Experimentally observed spectroscopic features in photodarkened Mn:$YAlO_3$ (1), their spectral positions (2), and assignment (3). Column 4—calculated positions of the energy levels obtained from the best fit of the experimental data and the Tanabe-Sugano diagram (calculated at $C/B=5$). $Dq=1240\,cm^{-1}$ and $B=524\,cm^{-1}$.

1	2	3	4
Experimentally observed spectral feature	Spectral position (experimental), cm^{-1}	Assignment of the transition	Spectral position (calculated from the Tanabe-Sugano diagram), cm^{-1}
Weak absorption and emission line at 1138 nm with satellite peaks, #1	8.79×10^3	$^3T_1(^3F)\rightarrow{}^1T_2(^1D)$	8.67×10^3
Wide absorption band #2	1.17×10^4	$^3T_1(^3F)\rightarrow{}^3T_2(^3F)$	1.14×10^4
Wide absorption band #3	1.55×10^4	$^3T_1(^3F)\rightarrow{}^3T_1(^3P)$	1.82×10^4
Wide absorption band #4	1.85×10^4		
Group of sharp weak absorption lines #5	20.57×10^3, 20.70×10^3, 21.43×10^3, 21.95×10^3	$^3T_1(^3F)\rightarrow{}^1A_1(^1G)$	1.82×10^4
Wide stuctureless absorption wing #6	$\approx2.6\times10^4$	$^3T_1(^3F)\rightarrow{}^3A_2(^3F)$	2.38×10^4

found in the crystal, Fig. 2. No emission in the same spectral range was observed at room temperature. The intensity of 1.14-μm emission was many orders of magnitude weaker than that of 715-nm emission. One of the strongest lines (1138 nm) in the 14-K emission spectrum corresponds to the strongest line in the 14-K absorption spectrum, Fig. 2. Apparently, this is the zero-phonon line of the electronic transition.

No other significant emission signals were found in the crystal.

The main features in the visible and near infrared absorption and emission spectra of the exposed Mn:$YAlO_3$ are summarized in Table I.

IV. DISCUSSION

4.1 Assignment of the absorption and emission features in Mn:$YAlO_3$

Assuming that the optical active center predominating in the absorption spectra of photoinduced Mn:$YAlO_3$ is Mn^{5+} (we will prove this assumption in this and the next subsections), its ground state, the ground state of the $3d^2$ ion in octahedral coordination, is $^3T_1(t_2^2)$ and the lowest ^1D singlet excited state is $^1T_2(t_2^2)$, see the Tanabe-Sugano diagram in Fig. 5. We attribute the 77-K emission and the 14-K emission and absorption at 1120-1180 nm, Fig. 2, to the intraconfigurational transition $^1T_2(t_2^2)\rightarrow{}^3T_1(t_2^2)$. A similar singlet→triplet sharp spectral line in the $7\times10^3-10\times10^3\,cm^{-1}$ range was observed in $3d^2$ ions in octahedral [V^{3+}:Al_2O_3,[11] V^{3+}:$Y_3Al_5O_{12}$,[12] V^{3+}:K_2NaScF_6,[13] V^{3+}:$Cs_2LiScCl_6$,[13] V^{3+}:$Cs_2LiInCl_6$,[13] V^{3+}:$Cs_2LiScBr_6$,[13] Ti^{2+}:$MgCl_2$ (Ref. 15)] and tetrahedral (Mn^{5+} in Y_2SiO_5,[7] apatites, spodiosites, and Li_3MO_4-type lattices[6,9]) coordination. This narrow-line absorption and emission definitely cannot belong to $Mn^{4+}(3d^3)$ ion, since Mn^{4+} emission in $YAlO_3$ is known to occur at ≈715 nm.[4] Besides, we are not aware of any $3d^3$ ion in laser related hosts that has emission beyond 1 μm. The strong line seen in the absorption and emission at 1136 nm ($\approx8.80\times10^3\,cm^{-1}$), Fig. 2, is apparently the zero-phonon line of the $^1T_2(t_2^2)\rightarrow{}^3T_1(t_2^2)$ transition. This is the shortest wavelength line in the 14-K emission spectrum. This implies the absence of anti-Stokes vibronic lines, which is not surprising at 14 K. We assume that in Fig. 2 the absorption lines at shorter wavelengths than 1136 nm and the emission lines at longer wavelengths than 1136 nm have vibronic origin or are due to the transitions involving spin-orbit components or crystal-field components

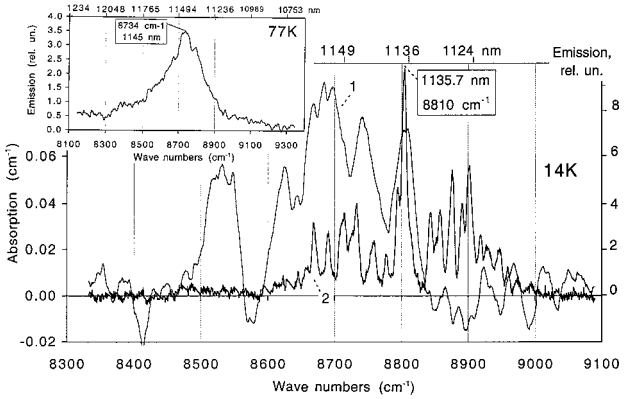

FIG. 2. Main frame: The 14-K emission spectrum (1) and absorption spectrum (2) of strongly exposed Mn(0.5%):$YAlO_3$. Inset: The same emission spectrum at 77 K.

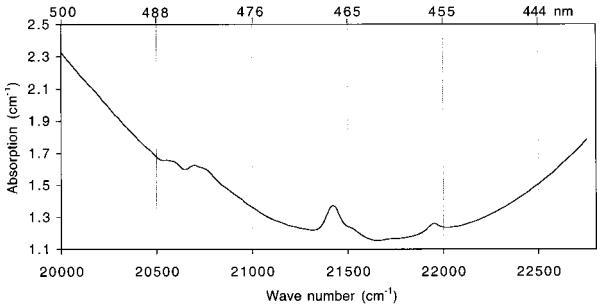

FIG. 3. The fragment of the 77-K absorption spectrum of exposed Mn:$YAlO_3$(**k**∥**c**, **E**∥**a**) recorded with higher resolution, 0.5 nm.

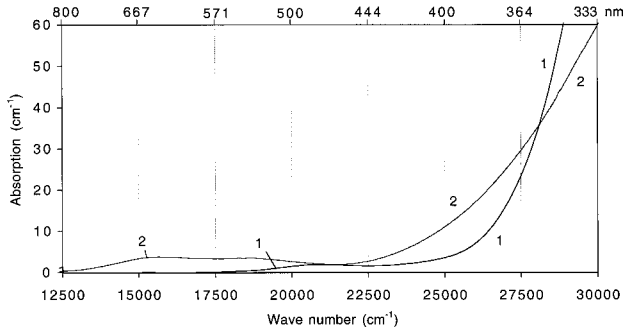

FIG. 4. Room-temperature absorption spectra of a thin ($l = 0.27$ mm) Mn:$YAlO_3$ sample; 1 - unexposed, 2 - strongly exposed by Ar^+ laser.

(in a symmetry lower than O_h) of the ground and excited states. To distinguish between the possible mechanisms above one should perform careful studies of the emission versus temperature, polarization, etc. Unfortunately, because of the extreme weakness of the $^1T_2(t_2^2) \rightarrow {}^3T_1(t_2^2)$ emission signal, this is not feasible. Thus, all the three possibilities above remain open. The relatively strong absorption lines seen above 1136 nm may imply the presence of several different types of Mn^{5+} centers in $YAlO_3$ (at cryogenic temperature). This explanation is consistent with the fact that three types of Mn^{4+} centers exist in Mn:$YAlO_3$ at 77 K.[4]

We assign absorption band #2 ($\approx 12\times10^3\,\mathrm{cm}^{-1}$), Fig. 1, to the spin-allowed transition $^3T_1(t_2^2) \rightarrow {}^3T_2(t_2e)$ and assign the poorly resolved band #4 ($\approx 25\times10^3\,\mathrm{cm}^{-1}$) to the transition $^3T_1(t_2^2) \rightarrow {}^3A_2(e^2)$. The $^3T_1(t_2^2) \rightarrow {}^3A_2(e^2)$ transition is a two-electron excitation and, as such, is expected to be weak. However, as it can be estimated from Fig. 4, the maximum intensity of photoinduced coloration at $\approx 26.3\times10^3\,\mathrm{cm}^{-1}$ is approximately 2.5 times higher than that at $15.5\times10^3 - 16.0\times10^3\,\mathrm{cm}^{-1}$. One can speculate that the relatively high intensity of this transition in respect to that of the $^3T_1(t_2^2) \rightarrow {}^3T_2(t_2e)$ transition, observed experimentally, is because its intensity-stealing ability may be enhanced by its proximity to CT bands. (In principle, one cannot exclude the possibility of $Mn^{5+} \rightarrow$oxygen CT in the vicinity of $26\times10^3\,\mathrm{cm}^{-1}$. However, the absorption intensity at $26\times10^3\,\mathrm{cm}^{-1}$ seems to be too small for a CT band.)

Bands #3 and #4 can be interpreted as the orbital components of the $^3T_1(t_2^2) \rightarrow {}^3T_1(t_2e)$ transition that is split due to some distortion of the Mn^{5+} octahedron. We believe that the splitting of the $^3T_1(t_2e)$ excited state is large, $\approx 2.5\times10^3\,\mathrm{cm}^{-1}$, giving rise to the bands at 15.5×10^3 and $18\times10^3\,\mathrm{cm}^{-1}$. In principle, if the symmetry of the Mn^{5+} site is low enough, the $^3T_1(t_2e)$ level can be split into three orbital components. If we assume that the spectral bands corresponding to these three components are polarization dependent, this would explain some variance ($<500\ \mathrm{cm}^{-1}$) in the maximum positions of the 15.5×10^3 and $18\times10^3\,\mathrm{cm}^{-1}$ bands experimentally observed in different polarizations, Fig. 1. In this scenario, the 15.5×10^3 and $18\times10^3\,\mathrm{cm}^{-1}$ bands apparently represent two strongest components in the $^3T_1(t_2e)$ splitting.

Note that the splitting of the excited $^3T_1$ state was observed in various crystals, for example, in $Cs_2LiScBr_6$ in trigonally distorted octahedral coordination ($\Delta E \approx 1000\ \mathrm{cm}^{-1}$) (Ref. 13) and in Ca_2VO_4Cl in tetrahedral coordination ($\Delta E \approx 3{,}700\,\mathrm{cm}^{-1}$).[6] The relatively smaller splitting, of the order of several hundred wave numbers, was observed in different crystals doped with $3d^2$ ions occupying (mostly trigonally) distorted octahedral sites [V^{3+}:Al_2O_3,[10,11] V^{3+}:$Y_3Al_5O_{12}$,[12] V^{3+}:$Cs_2LiScCl_6$,[13] V^{3+}:$Cs_2LiInCl_6$,[13] V^{3+}:$Cs_2LiScBr_6$,[13] and Tr^{2+}:$MgCl_2$ (Ref. 14)].

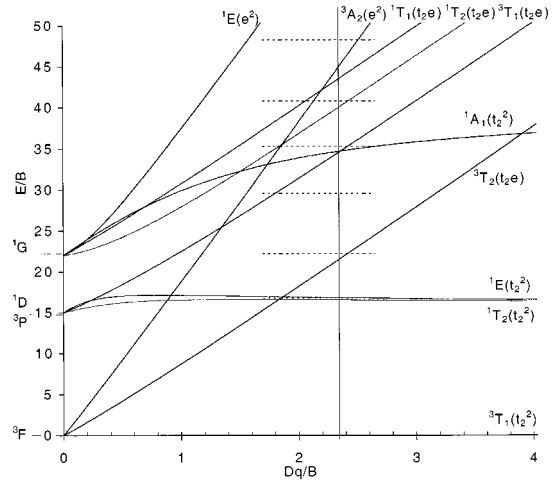

FIG. 5. The Tanabe-Sugano energy level diagram of a $3d^2$ system in an octahedral crystal field (calculated for $C/B = 5$). The horizontal dashed lines correspond to the experimentally measured energy positions of the states. The vertical line corresponds to the crystal field in Mn^{5+}:$YAlO_3$.

According to the Tanabe-Sugano diagram, Fig. 5, the energy of the level $^1A_1(t_2^2)$ has only very weak dependence on the crystal field (a similar situation also takes place in tetrahedral sites). Thus, one should expect that the spin forbidden transition between the triplet ground state and the excited state $^1A_1(t_2^2)$ will be seen in the absorption spectrum as a sharp-weak peak. The fine structure (in some cases not showing any regular energy intervals) attributed to the transition to the $^1A_1$ level was observed in $3d^2$ ions occupying octahedral sites [V^{3+}:Al_2O_3 (Ref. 10)] and tetrahedral sites [Mn^{5+}:Ca_2VO_4Cl,[6] Mn^{5+}:$YSiO_5$,[7] and Mn^{5+}:$Sr_5(VO_4)_3F$ (Ref. 9)] in the spectral range between the $^3T_2$ and $^3T_1$ absorption bands[7,9,10] or overlapping the $^3T_1$ absorption band.[6]

In our crystals, we did not see any sharp peaks in the spectral range between the $^3T_2$ and $^3T_1$ absorption bands. However, the set of unevenly spaced weak sharp lines was observed overimposed the high-energy wing of the $^3T_1(t_2e)$ band, Fig. 3. We tentatively associate these peaks with the transition $^3T_1(t_2^2) \rightarrow {}^1A_1(t_2^2)$. As it was suggested in Ref. 6, a fine structure in the broad-band absorption of Mn^{5+}:Ca_2VO_4Cl, that does not show any regular energy intervals, can be due to the mixing of the broad-band spin allowed transition and the ''groundstate'' $\rightarrow {}^1A_1(t_2^2)$ excitation. The same explanation can also be valid in the case of our experiment.

Thus, according to our spectroscopic measurements and assignments, the energy states in photodarkened Mn^{5+}:$YAlO_3$ correspond to those of Mn^{5+} in distorted octahedral coordination and are arranged in the following order:

$^1T_2(t_2^2)$, (not seen) $^1E(t_2^2)$, $^3T_2(t_2e)$, strongly split $^3T_1(t_2e)$, $^1A_1(t_2^2)$, and $^3A_2(e^2)$. Spin-forbidden and, hence, weak bands $^1T_2(t_2e)$ and $^1T_1(t_2e)$ (not seen in the spectra) are apparently located between the levels $^3T_1(t_2e)$, and $^3A_2(e^2)$. (Note that the distortion of Mn^{5+} containing octahedra in photodarkened $YAlO_3$ is not surprising. For example, the distortion of Mn sites in $YAlO_3$ was observed in the crystal codoped with Mn and Ce ions[5] and, at liquid nitrogen temperature, in single Mn-doped $YAlO_3$.[4])

4.2 Comparison to the Tanabe-Sugano diagram

In accordance with Refs. 22–24, we calculated the Mn^{5+} energy states (Tanabe-Sugano diagram) for an octahedral field in the cubic approximation. The calculation was done for the ratio of the Racah parameters C and B equal to $C/B=5$. According to Ref. 22, the ratio C/B in a large number of transition-metal ion-doped crystals is 4 to 5. Thus, we believe that $C/B=5$ is a reasonable first approximation applicable to Mn^{5+}:$YAlO_3$.

In the computational routine we varied the Racah parameter B and the crystal-field Dq, trying to get the best fit to the experimentally determined positions of the levels $^1T_2(^1D)$, $^3T_2(^3F)$, $^3T_1(^3P)$, and $^3A_2(^3F)$, Table I. In the minimization of the calculated/experimental energy mismatch for the $^3T_1(^3P)$ level, the two split components at $1.55\times10^4\,cm^{-1}$ and $1.85\times10^4\,cm^{-1}$ were taken (in two alternative calculations) with weights 2:1 and 1:2, since the degeneracy of unperturbed and unsplit $^3T_1(^3P)$ level is equal to three. At $C/B=5$, we obtained the best fit at $B=524\,cm^{-1}$ and $Dq=1240\,cm^{-1}$ when the 1.55×10^4 and $1.85\times10^4\,cm^{-1}$ bands are accounted with the weights 1:2. Correspondingly, the calculated position of the $^3T_1(^3P)$ level was much closer to $1.85\times10^4\,cm^{-1}$ than to $1.55\times10^4\,cm^{-1}$. The energy-level positions calculated at these values of the fitting parameters are reasonably close to those experimentally measured, Table I. The reasonably good agreement between the experiment and calculation confirms our statement that the observed spectroscopic features in photodarkened Mn:$YAlO_3$ are predominantly due to Mn^{5+} in distorted octahedral coordination (Al sites).

The largest mismatch between the calculations and experiment is in the energy of $^1A_1(^1G)$ level. However, it is known from the literature that the energy of this level is usually poorly reproduced from ligand-field calculations.[25,9] Since the maximum of the $^3A_2(^3F)$ absorption band is experimentally determined with rather low accuracy, Fig. 4, the obtained agreement between the calculated and experimental positions of this level is fair enough.

(Note that a slightly better fit of the experimental results and the Tanabe-Sugano diagram could be obtained at the larger value of C/B (with the optimum at $C/B\approx8$). The value of the parameter $C/B\approx8$ is close to that determined for Mn^{5+}:$Sr_5(PO_4)_3F$ in Ref. 9. However, a discussion about the physical reason for such a large value of C/B is beyond the scope of this paper.)

The determined parameter $Dq=1240\,cm^{-1}$ is less than that in Mn^{4+}:$YAlO_3$ [2115 cm^{-1} Ref. 4]. [However, it is still larger than Dq for some other $3d^2$ ions in octahedral coordination, 1018 cm^{-1} in Ti^{2+}:$MgCl_2$ (Ref. 15) and 1085 cm^{-1} in V^{3+}:$Cs_2LiScBr_6$.][13] The reason for the smallness of the parameter Dq in Mn^{5+}:$YAlO_3$ is not quite understood yet.

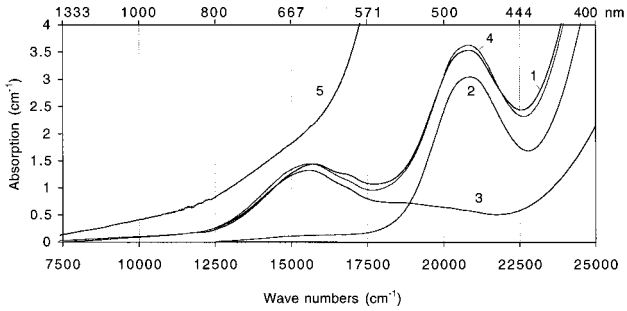

FIG. 6. Trace 1 - room-temperature absorption spectrum of the Mn(0.5%):Ce(0.4%):Ca(0.5%):$YAlO_3$; trace 2 - scaled absorption spectrum of Mn^{4+} in yellowish Mn(0.5%):$YAlO_3$; trace 3 - scaled absorption spectrum of Mn^{5+} in photodarkened Mn(0.5%):$YAlO_3$; trace 4 - the sum of traces 2 and 3. All ion concentrations are given according to the melt. Spectra are taken at $\mathbf{k}\|\mathbf{a}$ and $\mathbf{E}\|\mathbf{c}$. Trace 5 - absorption spectrum of Mn(0.5%),Ca(1%):$YAlO_3$.

4.3 Discussion of the energy position and luminescence from the $^1T_2$ level

Our tentative conclusion that the level $^1T_2(t_2^2)$ in Mn^{5+}:$YAlO_3$ is lower than $^3T_2(t_2e)$ is consistent with the absence of any detectable broad band luminescence in the crystal. In fact, the maximum of the $^1T_2(t_2^2)\rightarrow{}^3T_1(t_2^2)$ emission in Mn^{5+}:$YAlO_3$ is at $8.73\times10^3\,cm^{-1}$ and the maximum of the $^3T_1(t_2^2)\rightarrow{}^3T_2(t_2e)$ absorption is at $\approx12\times10^3\,cm^{-1}$. Apparently, even taking into account that $^3T_1(t_2^2)\rightarrow{}^3T_2(t_2e)$ is the interconfigurational transition and the actual energy gap between $^1T_2(t_2^2)$ and $^3T_2(t_2e)$ is less than $3.3\times10^3\,cm^{-1}$, the value of this energy gap is large enough to keep the population of the level $^3T_2(t_2e)$ negligibly small. Another possible reason preventing us from observation of the $^3T_2(t_2e)$ luminescence can be a strong nonradiative quenching of this level. As it is shown in Ref. 6, at room temperature the rate of the nonradiative quenching of the $^3T_2$ luminescence in Ca_2VO_4Cl is two orders of magnitude higher than the rate of the radiative process.

In many crystals with $3d^2$ ions substituted into octahedral sites the rate of the $^1T_2(t_2^2)\rightarrow{}^3T_1(t_2^2)$ transition is very low. For example, the radiative lifetime was estimated to be equal to 109 ms in Ti^{2+}:$MgCl_2$,[15] 18 ms in V^{3+}:$K_2LiScCl_6$,[13] 12 ms in $Cs_2LiInCl_6$ (site 1),[13] and 13.5 ms in V^{3+}:$Cs_2LiScCl_6$ (site 1).[13]

To estimate the radiative decay rate A at the $^3T_1(t_2^2)\rightarrow{}^1T_2(t_2^2)$ transition, we integrated the absorption spectrum in Fig. 6(b) ($\int k(\lambda)d\lambda$) and substituted the obtained value in the formula

$$A=\frac{(\int k(\lambda)d\lambda)8\pi cn^2}{N\overline{\lambda^4}},\qquad(1)$$

where $k(\lambda)$ is the absorption coefficient, $\overline{\lambda}$ is the central wavelength of the transition, c is the speed of light, n is the refraction index, and N is the concentration of Mn^{5+} ions. Taking into account that $\overline{\lambda}\approx1136\,nm$, $n\approx1.9$, and $N\approx5$

$\times 10^{18}\,cm^{-3}$ (the total Mn concentration in the crystal was $\approx 1\times 10^{19}\,cm^{-3}$ and Mn^{4+} concentration was approximately equal to a half of this value), we calculated A to be equal to $A \approx 310\,s^{-1}$ and $\tau = A^{-1} \approx 3.2\,ms$. The luminescence with such a long radiative lifetime can easily be quenched by various nonradiative processes, resulting in very low-luminescence quantum yield. Two possible nonradiative relaxation mechanisms for the singlet state in Mn^{5+}-doped crystals discussed in Ref. 6 are (i) direct nonradiative relaxation to the ground state when a normal (phonon) mode of a complex directly couples the excited state to the ground state (which would require a special symmetry of a phonon) and (ii) drain of the $^1T_2$ population via thermal coupling with the $^3T_2$ state followed by (radiative or nonradiative) relaxation of $^3T_2$. Apparently, this coupling should be rather weak. However, it can be strong enough to compete with very slow radiative relaxation of $^1T_2$. Note that very low-$^1T_2(t_2^2)$ emission intensity has been reported in V^{3+}:Al_2O_3 (Ref. 11) and V^{3+}:$Y_3Al_5O_{12}$ (Ref. 12) (octahedral sites in both cases).

V. STABILIZED MANGANESE 5+ VALENCE STATE IN Ca CODOPED CRYSTALS

As it was discussed in Ref. 5, Mn:$YAlO_3$ crystals codoped with Ce ions have pinkish color instead of yellowish color. Both Mn^{4+} and Mn^{3+} ions are seen in the absorption spectra of such crystals.[5] Apparently, Mn^{3+} ions appear in Ce codoped crystals as a result of the reaction $Ce^{3+}+Mn^{4+}\rightarrow Ce^{4+}+Mn^{3+}$.[5] In opposite, a $YAlO_3$ crystal (grown in oxidizing atmosphere) with nominal concentration (in the melt) of Mn ions equal to 0.5%, Ce ions equal to 0.4%, and Ca ions equal to 0.5% has dark grayish-brownish color. Its room-temperature absorption spectrum is shown in Fig. 6, trace 1. In the spectrum of Fig. 6 one can see Mn^{4+} absorption peak at $\approx 21\times 10^3\,cm^{-1}$ ($\approx 0.48\,\mu m$) and the peak characteristic to Mn^{5+} ions centered at $\approx 16\times 10^3\,cm^{-1}$ ($\approx 0.625\,\mu m$), compare with Fig. 1. Traces 2 and 3 in Fig. 6 are, correspondingly, the absorption spectra of Mn^{4+} ions in yellowish Mn(0.5%):$YAlO_3$ crystal and Mn^{5+} ions in photodarkened Mn(0.5%):$YAlO_3$ crystal scaled to fit (when added together) the absorption spectrum represented by trace 1. The perfect agreement of the experimental (trace 1) and fitted (trace 4) spectra in Fig. 6 is the evidence that the spectrum of Mn,Ce,Ca:$YAlO_3$ is the combination of Mn^{4+} absorption and Mn^{5+} absorption.

The dark coloration of Mn,Ce,Ca:$YAlO_3$ cannot be erased by heat. Thus, the presence of Ca ions stabilizes manganese 5+ valence state in the crystal. Under photoexcitation in the wavelength range below $\approx$550 nm the photoinduced Mn^{5+} absorption (additional to that present in as-grown crystal) appears in the sample. The photoinduced component of Mn^{5+} absorption can be easily erased by heat ($>250\,°C$), similar to the photocoloration in single Mn-doped $YAlO_3$.[1,2,4] However, chemically stabilized fraction of Mn^{5+} absorption in Mn,Ce,Ca:$YAlO_3$ is persistent.

The absorption spectrum of Mn(0.5%),Ca(1%):$YAlO_3$ (both concentrations are given according to the melt) is shown in Fig. 6, trace 5. One can see that in this crystal, Mn^{4+} and Mn^{5+} absorption bands are concealed under the wing of a very strong-absorption band centered in ultraviolet.

We hypothesize that divalent calcium ion, substituting trivalent yttrium ion in the crystal, forms a negatively charged center. Apparently, this negatively charged center helps in oxidation of Mn^{4+} to Mn^{5+} and stabilization of manganese in the 5+ valence state. One can also speculate that uncompensated negative Ca-based centers are responsible for the very strong-absorption band, probably belonging to some CT transition, in the short-wavelength range of the spectrum (Fig. 6, trace 5). Following this scenario, the CT absorption band disappears (Fig. 6, trace 1) when the effective concentration of ions serving as donors of electrons (Mn, Ce) is higher that the concentrations of Ca-based negative centers. Unfortunately, the lack of the knowledge of exact concentrations of Mn, Ce, and Ca ions in our crystals does not allow us to develop the model in greater detail.

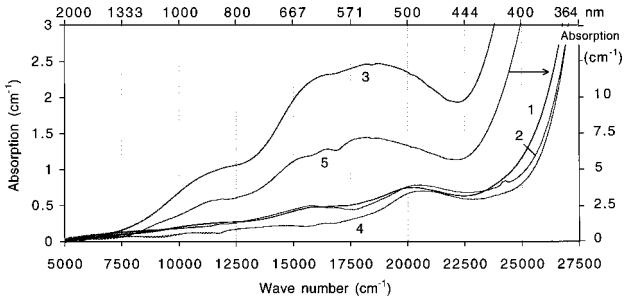

FIG. 7. Room-temperature absorption spectrum of nominally 2% Mn-doped $YAlO_3$ grown in reducing atmosphere. Traces 1 and 2 - slightly photoexposed crystal before the heat treatment; trace 3 - absorption of the overheated crystal (whole sample); trace 4 - absorption of the inner part of the overheated crystal; trace 5 - absorption of the (outer) thin slice of the overheated crystal (the scale for this trace is on the right-hand side of the plot). Trace 1 - **E**$\|$**c**, traces 2-5 - **E**$\|$**b**.

VI. STABILIZED Mn^{5+} IONS IN Mn:$YAlO_3$ GROWN IN REDUCING ATMOSPHERE

The sample of nominally 2% doped Mn:$YAlO_3$ grown in reducing atmosphere was brought to spectroscopic investigation several months after it was synthesized. During that time the crystal was occasionally exposed to room light. The crystal at this initial stage was lightly grayish. This color is typical to low-Mn-doped $YAlO_3$ crystals exposed to sunlight or room light. The polarized absorption spectra of the sample at this initial stage are shown in Fig. 7, traces 1 and 2. They show Mn^{4+} absorption band at $\approx 20.5\times 10^3\,cm^{-1}$, Mn^{5+} absorption band at $\approx 15.5\times 10^3 - 16\times 10^3\,cm^{-1}$ (compare with Fig. 1), the doublet of sharp weak lines at $\approx 24.3\times 10^3\,cm^{-1}$ (412 nm) (we attribute it to Mn^{2+} ions in yttrium positions, Ref. 5), and a wing of very strong-absorption band extending from ultraviolet. The Mn^{4+} absorption intensity in traces 1 and 2 is much smaller than that in nominally 0.5% Mn-doped $YAlO_3$ grown in oxidizing atmosphere (see Fig. 1). The Mn^{5+} absorption in the crystal, determining together with Mn^{4+} absorption very light grayish coloration of the sample, was weak too.

The exposure of the sample with green Ar^+ laser light did not produce any dramatic changes to the crystal color and spectrum, that was typical to Mn:$YAlO_3$ samples with low-Mn^{4+} concentration.

To erase Mn^{5+} grayish coloration in the crystal, we

heated the sample on the hot plate at ≈310 °C for approximately 10 min. (We routinely used the same type of heat treatment to erase photoinduced coloration in all our crystals grown in oxidizing atmosphere.) After this heating procedure the crystal became lightly yellowish with a slight trace of gray color. This was the expected result of the coloration erasing experiment. The change of the color to yellowish implied the reduction of Mn^{5+} absorption. However, the traces of gray coloration indicated that small Mn^{5+} concentration still remained in the crystal.

To remove the residual traces of Mn^{5+} absorption, we set up the sample on the hot plate and heated it at the second time at ≈460 °C for approximately 45 min. To our great surprise, the crystal after this second heat treatment became dark gray, much darker than it was initially before the first heating. This never happened to our Mn:$YAlO_3$ crystals grown in oxidizing atmosphere. The absorption spectrum of the overheated dark gray crystal (at **E**∥**b**) is shown in Fig. 7, trace 3. This spectrum is typical to Mn^{5+}, see Fig. 1. (The absorption spectrum of the overheated crystal in polarization **E**∥**c** was also characteristic to Mn^{5+}.)

We then cut two thin (<1 mm) slices from two opposite parallel faces of the sample and found that the inside volume of the crystal was light grayish yellowish, whereas the outer layer (several hundred of micrometers) was very dark. The spectrum of the inner part of the overheated crystal is shown in Fig. 7, trace 4. One can see that Mn^{5+} absorption in trace 4 is smaller than that in traces 1 and 2. The absorption spectrum of the thin outer slice of the crystal is shown in Fig. 7, trace 5. To calculate the absorption coefficient in trace 5, we accounted for the thickness of the slice, 0.83 mm. However, since the effective depth of the dark colorated layer was apparently less than 0.83 mm, the maximum absorption coefficient in the layer close to the crystal surface was even higher than that in trace 5. (Obviously, the absorption coefficient in trace 3 was calculated accounting for the total length of the crystal.)

The dark coloration in the thin skin layer stayed in the crystal permanently and could not be further removed by either short-time or long-time heating in the air.

Thus, as follows from this particular experiment, the short-time (≈10 min) heat treatment erases photoinduced Mn^{5+} coloration in Mn:$YAlO_3$ grown in reducing atmosphere, similarly to that it does in crystals grown in oxidizing atmosphere. In parallel with this, the permanent intense Mn^{5+} coloration appears in thin layer close to the crystal surface. This type of thin skin coloration has never been observed after the heat treatment in Mn:$YAlO_3$ crystals grown in oxidizing atmosphere.

One can hypothesize that intense permanent coloration in thin outer layer of the crystal (grown in reducing atmosphere) is due to diffusion of oxygen into the crystal during the heat treatment. The excess of oxygen oxidizing Mn^{4+}($Mn^{4+}\rightarrow Mn^{5+}$) and stabilizing Mn^{5+} can effectively play the role of negative Ca-based centers discussed in Sec. V. More studies of various lattice defects are needed to answer the question why oxygen diffusion at relatively low temperature (310–460 °C) takes place in Mn:$YAlO_3$ grown in reducing atmosphere and does not occur in Mn:$YAlO_3$ grown in oxidizing atmosphere.

VII. SUMMARY

In the present paper we studied spectroscopic properties of photoinduced color centers in Mn:$YAlO_3$ and showed that they correspond to those of Mn^{5+} ions in octahedral sites. We assign the main features observed in the absorption and emission spectra of strongly photoexposed Mn:$YAlO_3$ to the following excited energy states: $^1T_2(t_2^2)$, $^3T_2(t_2e)$, strongly split $^3T_1(t_2e)$, $^1A_1(t_2^2)$, and $^3A_2(e^2)$. We attribute the strong splitting of the $^3T_1(t_2e)$ excited state to the distortion of Mn^{5+} octahedral site. The character of the distortion of Mn^{5+} containing octahedron in Mn:$YAlO_3$ apparently changes with temperature. We discuss the possible position of Mn^{5+}:$YAlO_3$ in Tanabe-Sugano diagram and the reasons for low-quantum yield of Mn^{5+} emission. We also describe two examples when Mn^{5+} ions are chemically stabilized in Mn:$YAlO_3$ as a result of codoping of the crystals with Ca ions or annealing of the crystals (grown in reducing atmosphere) in air at 310–460 °C.

Note added in proof. The orientation of the crystallographic axes in $YAlO_3$ crystals was studied using Rigaku x-ray set up with an attachment for Laue measurements. (This study was done by Hands P. Jenssen of CREOL, University of Central Florida.) This measurements has shown that the axis **a** is oriented along the boule. All the $YAlO_3$ crystals grown have the oval cross section. The larger oval radius points in the **c** direction and the smaller radius points in the **b** direction (*Pbnm* notation). The fact that the lattice parameters ''c'' is larger than the lattice parameter ''b'' is in line with the later observation. The NMR studies of Mn:$YAlO_3$ have shown that the Laue determination of the crystallographic axes is in agreement with that done in Ref. 26. (The NMR studies were done by Natalia Noginova. The results will be published separately.) Note that in our several previous publications.[1,2,4,5,27] following Ref. 28, we determined the crystallographic axes in $YAlO_3$ boules based on the orientation of twin planes and characteristic rhombic dislocation pits that could be seen on specially oriented $YAlO_3$ wafers after etching. Unfortunately, that determination was not correct. In publications cited in Refs. 1,2,4,5,27 the axes orientations should be corrected as follows $\mathbf{a}_{old}\rightarrow\mathbf{c}_{new}$, $\mathbf{b}_{old}\rightarrow\mathbf{a}_{new}$, $\mathbf{c}_{old}\rightarrow\mathbf{b}_{new}$. (Her subscript ''old'' refers to the erroneous determination used in Refs. 1,2,4,5,27 and subcript ''new'' refers to the correct axes determination done with the x-ray Laue method.)

ACKNOWLEDGMENTS

This work was partially supported by the AFOSR/BMDO Grant No. F49620-98-1-0101, DOE Grant No. DE-FG01-94EW 11493, and NSF CREST project, Cooperative Agreement No. HRD-9805059. The authors want to express the special thanks to Hans P. Jenssen of CREOL, UCF, for the x-ray Laue determination of the crystal axes. The authors also thank Carl E. Bonner for the help with experiments.

*Electronic address: mnoginov@nsu.edu

[1] G. B. Loutts, M. Warren, L. Taylor, R. R. Rakhimov, H. R. Ries, G. Miller III, M. A. Noginov, M. Curley, N. Noginova, N. Kukhtarev, H. J. Caulfield, and P. Venkateswarlu, Phys. Rev. B **57**, 3706 (1998).

[2] M. A. Noginov, N. Noginova, M. Curley, N. Kukhtarev, H. J. Caulfield, P. Venkateswarlu, and G. B. Loutts, J. Opt. Soc. Am. B **15**, 1463 (1998).

[3] The evolution of an electron released in the process of photoionization is beyond the scope of this paper and will be discussed elsewhere.

[4] M. A. Noginov and G. B. Loutts, J. Opt. Soc. Am. B **16**, 3 (1999).

[5] M. A. Noginov, G. B. Loutts, and M. Warren, J. Opt. Soc. Am. B **16**, 475 (1999).

[6] U. Oetliker, M. Herren, H. U. Güdel, U. Kesper, C. Albrecht, and D. Reinen, J. Chem. Phys. **100**, 8656 (1994).

[7] U. Hömmerich, H. Eilers, W. M. Yen, and H. R. Verdun, Chem. Phys. Lett. **213**, 163 (1993).

[8] M. Herren, H. U. Güdel, C. Albrecht, and D. Reinen, Chem. Phys. Lett. **183**, 98 (1991).

[9] S. Kück, K. L. Schepler, and B. H. T. Chai, J. Opt. Soc. Am. B **14**, 957 (1997).

[10] D. S. McClure, J. Chem. Phys. **36**, 2757 (1962).

[11] Z. Goldschmidt, W. Low, and M. Foguel, Phys. Lett. **19**, 17 (1965).

[12] M. J. Weber and L. A. Riseberg, J. Chem. Phys. **55**, 2031 (1971).

[13] C. Reber, H. U. Güdel, G. Meyer, T. Shield, and C. Daul, Inorg. Chem. **28**, 3249 (1989).

[14] D. R. Wilson, D. H. Brown, and W. E. Smith, Inorg. Chem. **25**, 898 (1986).

[15] S. M. Jacobsen, H. U. Güdel, and C. A. Daul, J. Am. Chem. Soc. **110**, 7610 (1988).

[16] L. D. Merkle, A. Pinto, H. R. Verdún, and B. McIntosh, Appl. Phys. Lett. **61**, 2386 (1992).

[17] L. D. Merkle, H. R. Verdún, and B. McIntosh, in *Advanced Solid-State Lasers*, edited by A. A. Pinto and T. Y. Fan, OSA Proceedings Series Vol. 15 (Optical Society of America, Washington, D.C., 1993), pp. 310–314.

[18] L. D. Merkle, Y. Guyot, and B. H. T. Chai, J. Appl. Phys. **77**, 474 (1995).

[19] R. Diehl and G. Brant, Mater. Res. Bull. **10**, 85 (1975).

[20] R. D. Shannon, Acta Crystallogr., Sect. A: Cryst. Phys., Diffr., Theor. Gen. Crystallogr. **A32**, 751 (1976).

[21] R. G. Burns, *Mineralogical Applications of Crystal Field Theory*, 2nd ed. (Cambridge University Press, Cambridge, 1993), p. 551.

[22] B. Henderson and G. F. Imbusch, *Optical Spectroscopy of Inorganic Solids* (Clarendon Press, Oxford, 1989), p. 645.

[23] Y. Tanabe and S. Sugano, J. Phys. Soc. Jpn. **9**, 753 (1954).

[24] Y. Tanabe and S. Sugano, J. Phys. Soc. Jpn. **9**, 766 (1954).

[25] C. K. Jørgensen, *Orbitals in Atoms and Molecules* (Academic, New York, 1962).

[26] D. P. Burum, R. M. Macfarlane, R. M. Shelby, and L. Mueller, Physics Letters, **91A**, p. 465 (1982).

[27] N. Noginova, W. Lindsay, M. A. Noginov, G. B. Loutts, and L. Mattix, JOSA B **16**, 754 (1999).

[28] B. Cockayne, B. Lent, J. S. Abel, and P. M. Marquis, J. Mater. Sci. **10**, 1874 (1975).